UNIVERSITY OF CALIFORNIA SAN DIEGO

Improvement of Electrocardiography for Clinical Diagnosis

A Thesis submitted in partial satisfaction of the
requirements for the degree Master of Science

.

in

Electrical Engineering
(Medical Devices and Systems)

by

Ellie Sadatian

Committee in charge:

Professor Tse Nga Ng, Chair
Professor Duygu Kuzum
Professor Sheng Xu

2020

The Thesis of Ellie Sadatian is approved, and it is acceptable in quality and form for publication on microfilm and electronically:

_____

_____

_____
Chair

University of California San Diego

2020

DEDICATION

To my parents and brother.

TABLE OF CONTENTS

Signature Page iii

Dedication iv

Table of Contents v

List of Figures vii

List of Tables ix

Acknowledgements x

Vita xi

Abstract of the Thesis xii

Chapter 1 (Electrocardiography Improvement Method) 1

1.1 Introduction 1

1.2 Methods 5
1.2.1 Electrode Fabrication 5
1.2.2 Hydrogel Preparation 7

1.3 Characterization 9
1.3.1 Dry Electrode Characterization 9
1.3.2 Hydrogel Characterization 16

1.4 Conclusion and Future Directions 23

1.5 References 23

Chapter 2 (Printing of the Passivation Layer in an All-Printed Supercapacitor) 25

2.1 Introduction 25

2.2 Methods 26

2.3 Effectiveness of the Passivation Layer 28

2.4 Conclusion and Future Directions 29

2.5 References 30

Chapter 3 (Capacitive Pressure Sensing via Distributed Multi-Channel Frequency-Modulation-Based System) 31

3.1 Introduction 31
3.2 Front-End Circuit Design 32
3.3 Experimental Testbed and Pressure Detection 33
3.4 Conclusion and Future Directions 36
3.5 References 36

LIST OF FIGURES

Figure 1.1. The cardiac conduction system; SA node, AV node, bundle of his, and Purkinje fibers. 1

Figure 1.2. ECG waveform genesis. 2

Figure 1.3. The precordial leads (V_1-V_6). 3

Figure 1.4. The design of the V_3-V_6 electrodes band.....4

Figure 1.5. The layers of the fabricated prototype: (a) adhesive tape, (b) backbone layer, (c) electrode layer, and (d) insulation layer.....6

Figure 1.6. A fabricated V_3-V_6 band.....7

Figure 1.7. Ionic crosslinking between Calcium ions and PVA chains.....7

Figure 1.8. The electrode structure and the hydrogel placement. The hydrogel covers the exposed electrode area. 8

Figure 1.9. (a) Fabricated dry electrode before (left) and after stretch (right). (b) The resistance of the dry electrode as %strain increases. 9

Figure 1.10. 12-lead ECG data collected using fabricated dry electrodes. 11

Figure 1.11. 12-lead ECG data collected using fabricated electrodes at ~30% strain for V_3-V_6 band.....12

Figure 1.12. 12-lead ECG data collected using commercial electrodes. 13

Figure 1.13. 3-lead ECG measurements of commercial, fabricated, and stretched fabricated electrodes are shown from left to right respectively.....15

Figure 1.14. The signal and noise data selection for SNR calculation per heartbeat.....16

Figure 1.15. (a) The PEIS measurements (b) and resistance of the hydrogel as the $CaCl_2$ concentration is increased.....17

Figure 1.16. (a) The PEIS measurements (b) and residual weight of Hydrogel 1 as a function of drying time.....18

Figure 1.17. PEIS measurements of Hydrogels 1-5.....19

Figure 1.18. (a) PEIS measurement for V_3 electrodes coated with Hydrogel 3 and placed on the skin and (b) its equivalent circuit model.....20

Figure 1.19. (a) PEIS measurement for V_3 dry electrodes placed on the skin and (b) its equivalent circuit model. 20

Figure 1.20. 3-lead ECG measurements of commercial and fabricated dry and with-hydrogel electrodes are shown from left to right respectively. 22

Figure 2.1. Printed supercapacitor layers. 25

Figure 2.2. Non-passivated device over time. 26

Figure 2.3. Voltera V-One PCB printer. 26

Figure 2.4. The two main steps for printing of the passivation layer. (a) The outer layer (left) is printed first, and then (b) the supercapacitor surface is covered. 27

Figure 2.5. The effectiveness of the printed passivation layers for devices with (a) PTFE, (b) PV alcohol, (c) PV acetate, (d) PV acetate & electrolyte, and (e) CE as their preserving material shown in terms of CV measurements. 28

Figure 3.1. Schematic of the cross-coupled current reuse LC tank voltage-controlled oscillator used for FM carrier generation. 32

Figure 3.2. Schematic of the bandpass amplifier used for signal combination on the FM-FDM bus. 32

Figure 3.3. Assembled sensor PCB. 33

Figure 3.4. Experimental testbed. 34

Figure 3.5. Measurement results under increasing and decreasing pressure applied to sensor. ...35

Figure 3.6. (a) Measurement results for two channel test and (b) its overall system setup. 36

LIST OF TABLES

Table 1.1. SNR values of the commercial electrodes placed in the positions of V_3 through V_6 and electrodes V_3-V_6 for the fabricated band before and after stretch. 16

Table 1.2. The recipes used for hydrogel trials as concentrations of PEDOT:PSS and $CaCl_2$ was varied in the solutions containing 0.5g of PVA dissolved in 4.5g of DI water. 18

Table 1.3. SNR values of V_3-V_6 electrodes coated with hydrogel for the fabricated band. 21

ACKNOWLEDGEMENTS

I would like to thank Professor Tse Nga (Tina) Ng and express my utmost gratitude for her guidance, feedback, and extraordinary mentorship throughout my master's study. She has been a source of motivation, inspiration, and knowledge. I would like to also thank her for believing in me and providing me with career-changing opportunities and for her continuous encouragement and support. I am very grateful to have had her as a mentor.

I would like to also thank Professor Truong Nguyen, who also believed in my potential and ability to pursue a graduate degree.

I am also grateful to Dr. Myeong-Lok Seol, Dr. Jin-Woo Han, and Dr. M. Meyyappan for their outstanding mentorship during my internship at NASA Ames Research Center and for providing me with an opportunity to gain valuable skills in the field of printed electronics.

Additionally, I want to acknowledge my teammates Thy Le, Kevin Ko, and Dr. Julian Warchall for their mutual assistance and Dr. Harinath Garudadri and Professor Tse Nga Ng for their guidance throughout the Capacitive Sensing Project.

And last, but certainly not the least, I would like to thank my brother, Dan, and my parents who have always supported me and helped me keep on going through the hardest of times, and my friends Katherine, Nasrin, and Eric, who have always been there for me and kept me motivated.

Chapter 2, in full, is the reprint of the material as it appears in the publication: Myeong-Lok Seol, Ellie Sadatian, Seohyeon Jang, Curtis Hill, Inho Nam, Jin-Woo Han, and M. Meyyappan, "Printing of a Passivation Layer for the Protection of Printed Supercapacitors", *ACS Appl. Electron. Mater.* 2, 3643 (2020). The thesis author is the primary author of this thesis and second author of this paper.

VITA

2018 B.S., Electrical Engineering, University of California San Diego

2020 M.S., Electrical Engineering, University of California San Diego

PUBLICATIONS

Myeong-Lok Seol, Ellie Sadatian, Seohyeon Jang, Curtis Hill, Inho Nam, Jin-Woo Han, and M. Meyyappan, “Printing of a Passivation Layer for the Protection of Printed Supercapacitors”, *ACS Appl. Electron. Mater*. 2, 3643 (2020).

ABSTRACT OF THE THESIS

Improvement of Electrocardiography for Clinical Diagnosis

by

Ellie Sadatian

Master of Science in Electrical Engineering
(Medical Devices and Systems)

University of California San Diego, 2020

Professor Tse Nga Ng, Chair

Continuous monitoring of the heart rhythm and electrophysiology is a vital biosensing ability that is routinely utilized by hospitals around the world. This process is made available by detecting electrical activity of the heart during the cardiac cycles using electrodes placed on the surface of the skin; hence producing an electrocardiogram (ECG). Due to the urgency of care, specifically in the emergency rooms, rapid and accurate application of such biosensors are crucial.

To address this need, an elastic multi-electrode fabric-based band will be prototyped wherein ECG electrodes and their connecting wires are integrated.

Chapter 1 focuses on fabrication and characterization of multi-electrode bands using screen-printing for both dry-electrodes and hydrogel-coated electrodes. Then ECG data is collected for the fabricated electrodes and compared to commercial electrodes in terms of signal-to-noise ratio (SNR) and waveform. The results indicated that the fabricated multi-electrode band has a slightly lower SNR in comparison to the commercial electrode, but it can be a suitable candidate for ECG recordings.

Although screen-printing of electrodes allows for low-cost and rapid manufacturing of such electrodes, the fabrication process can be more automated using printing. In Chapter 2, printing of a passivation layer will be established for an all-printed supercapacitor, and the technology used for printing of this device can be directly transferred to ECG electrode fabrication. Chapter 3, demonstrates a distributed multi-channel frequency-modulation-based data acquisition system for a capacitive pressure sensing transducer; however, this technology is sensor-type-agnostic and can be applied to other biosensors, such as for ECG recordings.

Chapter 1

Electrocardiography Improvement Method

1.1 Introduction

A heartbeat is the result of a series of contractions in the cardiac muscle which generate the mechanical force that is needed to pump the blood through the circulatory system. These contractions are due to generation and propagation of electrical impulses by specialized muscle cells and through the cardiac conduction system. The electrical impulse is activated in a cluster of pacemaker cells, known as the sinoatrial (SA) node which then travels to the atrioventricular (AV) node, bundle of His, and through the right and left bundle branches to the Purkinje fibers respectively (**Figure 1.1**). The resulting potential changes in the cells create time-varying dipoles

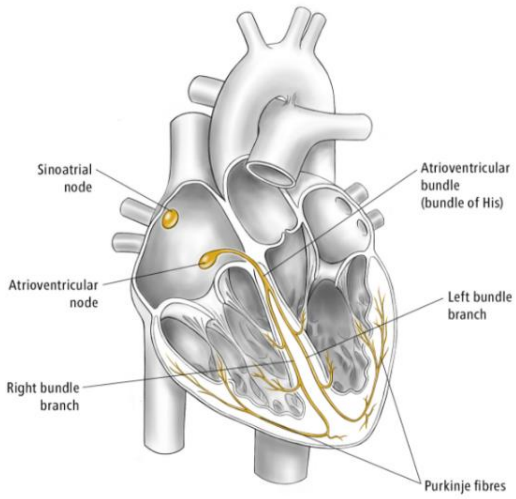

Figure 1.1. The cardiac conduction system; SA node, AV node, bundle of his, and Purkinje fibers.[1]

that can be summarized as a "dominant vector" describing the overall direction of the electrical impulse.[2] A projection of this vector can be detected in terms of potential difference between

electrodes placed on the surface of the body. The time-dependent potential readings provided by these surface electrodes, known as electrocardiogram (ECG), provides valuable information regarding the morphology and duration of the stages of the heartbeat.

An ECG waveform can represent the heart's electrical activity during a cardiac cycle as shown in **Figure 1.2**. Starting at rest, the membrane potential of the cardiac cells is then rapidly increased (depolarized) in the atria as the SA node initializes the heartbeat. This is followed by the electrical impulse reaching the AV node and subsequently ventricular depolarization occurs as the signal travels further in the cardiac conduction system. The ventricles then repolarize, and the cardiac cells return to rest again.

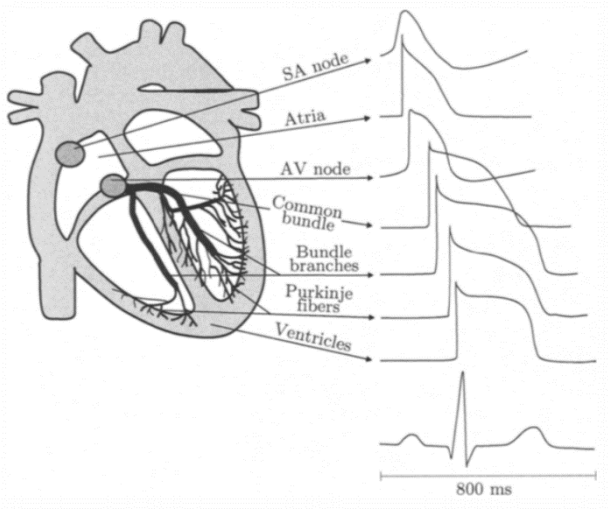

Figure 1.2. ECG waveform genesis.[2]

The most common ECG acquiring system is a 12-lead ECG recording setup, which is commonly used by healthcare professionals. There is a total of 10 electrodes generally used for this setup which consists of limb electrodes (V_{LA}, V_{LL}, V_{RA}, and V_{RL} that are placed on the left arm, left leg, right arm, and right leg respectively) and precordial electrodes (V_1, V_2, V_3, V_4, V_5,

and V_6 which are placed an front of the heart as shown in **Figure 1.3**). Using these 10 electrodes, three main lead configurations can be formed; (1) bipolar limb leads, (2) augmented unipolar limb leads, and (3) precordial leads. The bipolar limb leads I, II, and III are calculated using the simple potential differences as shown in equations (1-1) to (1-3).

$$I = V_{LA} - V_{RA} \quad (1\text{-}1)$$

$$II = V_{LL} - V_{RA} \quad (1\text{-}2)$$

$$III = V_{LL} - V_{LA} \quad (1\text{-}3)$$

The augmented unipolar limb leads are calculated as

$$aVR = V_{RA} - \frac{V_{RA} + V_{LL}}{2} \quad (1\text{-}4)$$

$$aVL = V_{RA} - \frac{V_{RA} + V_{LL}}{2} \quad (1\text{-}5)$$

$$aVF = V_{LL} - \frac{V_{LA} + V_{RA}}{2} \quad (1\text{-}6)$$

and can monitor the heart at a 30° shift with respect to the direction of the bipolar limb leads. The precordial leads are acquired from V_1-V_6 electrodes and provide a more comprehensive view of the heart. Electrodes V_1 and V_2 must be placed in the fourth intercostal space to the right and left of sternum respectively. Electrode V_3's position is midway between V_2 and V_4 where V_4 is placed in the fifth intercostal space and in the mid-clavicular line. V_5 and V_6 must be placed on the same horizontal level as V_4 and on the anterior axillary line and mid-axillary line respectively.

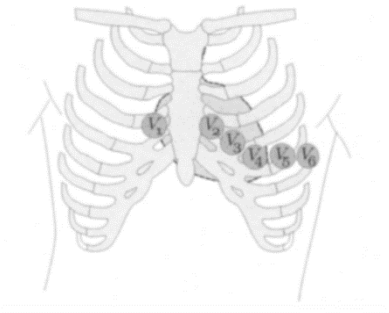

Figure 1.3. The precordial leads (V_1-V_6).[2]

Considering that placement of ten electrodes (or nine electrodes, as the placement of ground RL electrode is not necessary for obtaining a 12-lead ECG) can be rather time-consuming in emergency settings and can also introduce a number of possible user errors and electrode misplacements, it is crucial to improve the ECG electrode placement process to avoid over- or under-diagnosis. Among the ten electrodes, the ECG is more affected by the accuracy of placement of precordial leads rather than the limb electrodes.[3] The limb electrodes must be placed on the correct limbs and at least 15 cm away from the heart, but their precise location does not significantly affect the ECG.[3] This is while prominent changes in ECG morphology can be observed if the precordial leads are misplaced beyond 2 cm of their designated locations.[4] In a study performed by Kerwin et al., precordial electrode placements performed by alert and trained technicians were inaccurate by often 2-3cm.[5] This inaccuracy was more prominent when the electrodes were placed on female subjects; inaccurate lead placement were observed on 50 to 60% of male subjects and 80 to 85% of female subjects.[5]

To minimize the variations in single electrode placement, an electrode band was prototyped with electrodes V_3 to V_6. The electrodes were integrated into a stretchable fabric band, as shown in **Figure 1.4** in order to speed the process and improve electrode placement accuracy. The fabric and electrodes are required to stretch to at least 30% higher than their initial length to account for chest volume expansions during regular breathing. The distance between these electrodes were

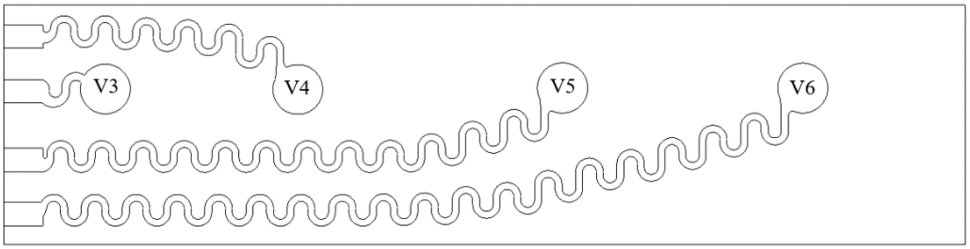

Figure 1.4. The design of the V_3-V_6 electrodes band.

experimentally determined on a volunteer with written consent, and the ECG recordings for SNR calculation were also performed on the same volunteer.

1.2 Methods

The fabrication of the stretchable ECG electrode band can be divided into two sections; dry electrodes and hydrogel preparation. The first section consists of fabrication of the basis for data collection and stretching ability of the dry electrodes. In the second section, a conductive adhesive hydrogel will be made for the surface of the electrodes to insure surface contact with the skin for long time measurements.

1.2.1 Electrode Fabrication

A prototype of the stretchable electrodes was developed by screen-printing, and it consists of four layers as shown in **Figure 1.5**. The first layer (**Figure 1.5 (a)**) is a clinical grade kinesiology tape (SpiderTech Inc., Ontario, Canada) that is uniaxially stretchable. The tape contains a serpentine-patterned adhesive layer on fabric. The following three layers were coated through a stencil and cured at 90°C for 10 minutes each. The stencil pattern was designed on AutoCAD and cut using Silhouette Cameo 3 on 152.4-micron (6-mil) PET.

The second layer (**Figure 1.5 (b)**) is composed of EcoFlex™ 00-10 rubber[6] (EcoFlex-10), which is a clear platinum-catalyzed silicone. This layer is used as the backbone which improves the mechanical stability and provides a uniform surface for the electrode layer coating, as inspired by Yin et. al.[7] Additionally, it creates a strong adhesion between the fabric and electrode as EcoFlex-10 is “tacky” to the touch once cured.

The third layer, as shown in **Figure 1.5 (c)**, is the conductive layer with the same stencil pattern as the backbone layer. This layer consists of the main ECG electrode and the conducting wire in a serpentine pattern to allow for the conductor to stretch to a higher degree without disintegration. The electrode is composed of silver/silver chloride ink (E2414, Ecron) mixed with EcoFlex-10 at 94:6 weight ratio to allow for more stretch in the conductor.[8]

The last layer insulates the wires and has a thicker serpentine pattern to ensure coverage, **Figure 1.5 (d)**. This layer is also responsible for providing shielding against the high voltage of the defibrillator which can range from 2500-5000 V. The material used for shielding is EcoFlex-10 which has a dielectric strength of > 13.78 V/micron (350 volts/mil). Therefore, the ability of

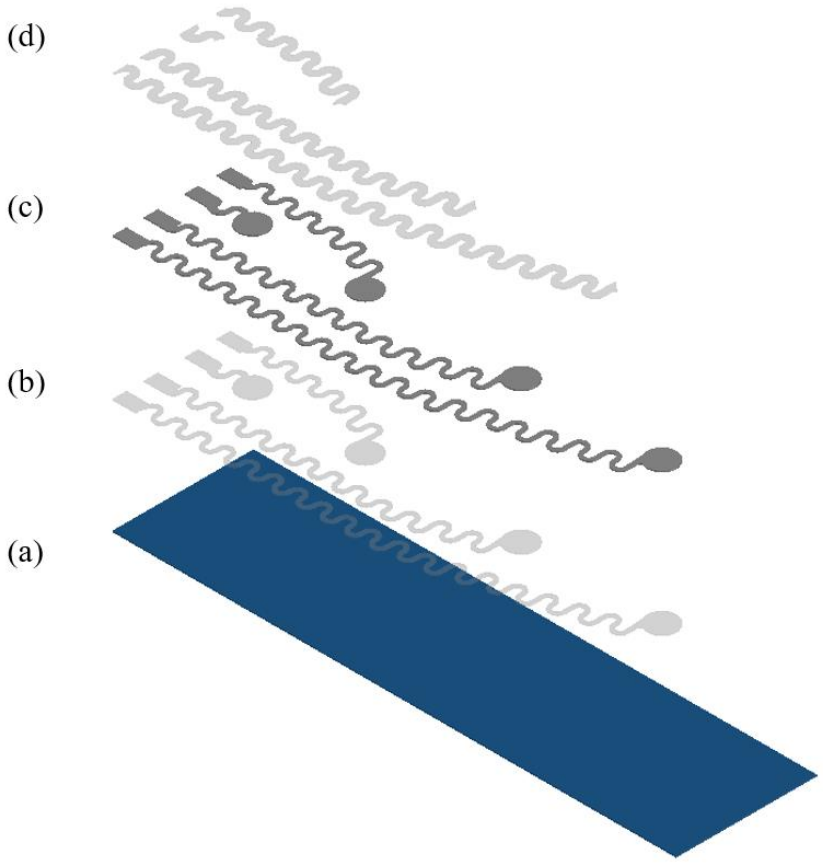

Figure 1.5. The layers of the fabricated prototype: (a) adhesive tape, (b) backbone layer, (c) electrode layer, and (d) insulation layer.

this layer to withstand higher voltages is dependent on its thickness, 2100 V per stencil. **Figure 1.6** shows the top view of a complete fabricated band containing V_3 to V_6 electrodes.

Figure 1.6. A fabricated V_3-V_6 band.

1.2.2 Hydrogel Preparation

The hydrogel is used to cover the surface of the electrodes to ensure a well-maintained surface contact with the skin during ECG acquisition; therefore, the hydrogel must be conductive and have adhesive properties. The hydrogel is composed of Polyvinyl Alcohol (PVA), Calcium Chloride ($CaCl_2$), and Poly(3,4-ethylenedioxythiophene) Polystyrene Sulfonate (PEDOT:PSS). Covalently crosslinked PVA hydrogels are widely used due to water-solubility of PVA and Young's modulus and deformation properties that are similar to that of biological tissues[9]; however, they are not conductive or adhesive. On the other hand, a divalent metallic salt such as

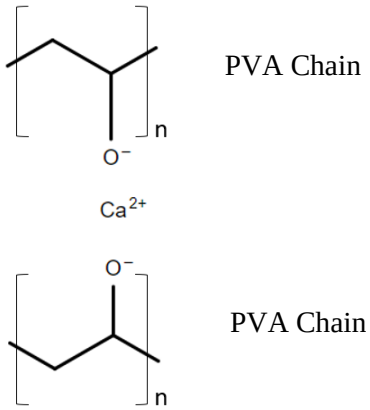

Figure 1.7. Ionic crosslinking between Calcium ions and PVA chains.

$CaCl_2$ can form a weak ionic cross-link with PVA chains (**Figure 1.7**), which results in a "sticky" hydrogel with an excellent water-holding ability due to Calcium ions[10]. PEDOT:PSS was also added as this polymer has a very high electrical conductivity which is desired, to lower the resistance during ECG acquisition.

The hydrogel preparation was performed over the course of several trials as characterized in section 1.3.2. The hydrogel with the lowest resistance was prepared by first dissolving 0.5g of PVA (molecular weight of 31000-50000, 98-99% hydrolyzed, purchased from Sigma Aldrich) in 4.5mL of DI water (10wt% PVA) at 85°C for over 16 hours until completely dissolved. 1.546g of PEDOT:PSS was then added to the solution under constant stirring for 2 hours at room temperature. The PEDOT:PSS used was an aqueous dispersion in water with 1.0-1.3% solid content (Clevios™ PH 1000) purchased from Heraeus. $CaCl_2$ (anhydrous, ≥97% assay, purchased from Sigma Aldrich) was next added to the solution at 2.1g and mixed for 2 hours at room temperature. The solution is stencil coated on the electrodes as shown in **Figure 1.8**. At room

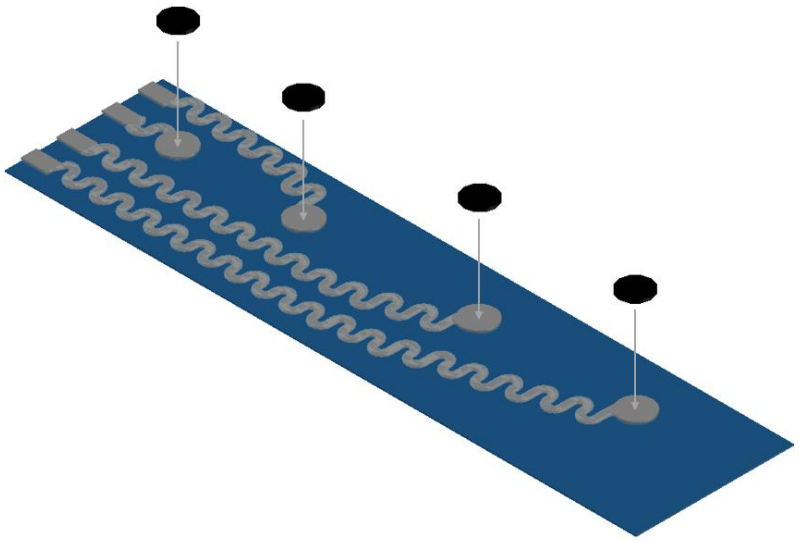

Figure 1.8. The electrode structure and the hydrogel placement. The hydrogel covers the exposed electrode area.

temperature, the hydrogel requires >4 weeks to be fully crosslinked and turn from a liquid to an adhesive hydrogel with the current formulation.

1.3 Characterization

The fabricated electrodes were used to make ECG measurements for the cases of:

1. dry electrodes before and after a stretch of up to 30% for V_3-V_6 band
2. and electrodes with hydrogel.

Characterization of this data is therefore separated into dry electrodes and electrodes with hydrogel sections.

1.3.1 Dry Electrodes Characterization

The resistance of a fabricated dry electrodes at its original length and as the %strain increases (**Figure 1.9 (a)**) was measured using a voltmeter. As shown in **Figure 1.9 (b)** the results of this experiment showed that the resistance increases overall as the electrode serpentine pattern is stretched and %strain increases. Additionally, it is noteworthy to mention that the resistance of the electrode has increased by ~18% at ~30% strain.

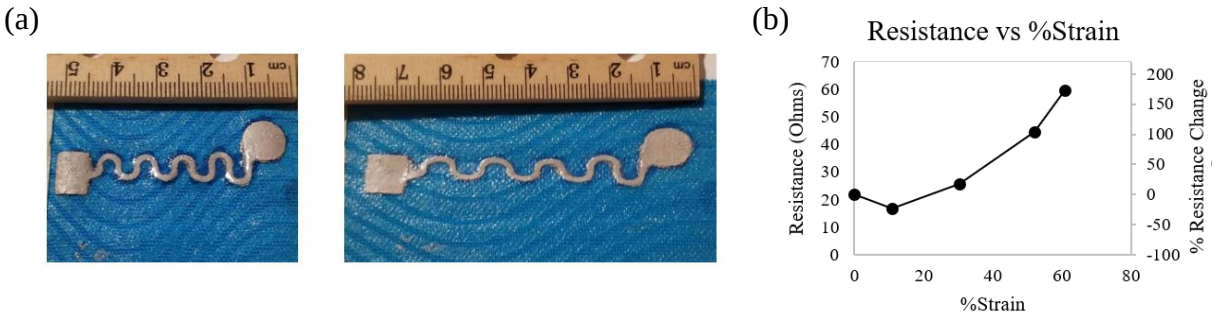

Figure 1.9. (a) Fabricated dry electrode before (left) and after stretch (right). (b) The resistance of the dry electrode as %strain increases.

The performance of the fabricated dry electrodes for ECG detection was then assessed using 12-lead and 3-lead measurements. The 12-lead ECG measurements were performed using 9 electrodes placed on RA, LA, LL, V_1, V_2, and the V_3-V_6 band before and after stretching of V_3-V_6 band up to ~30% of their original wire lengths, shown in **Figure 1.10** and **Figure 1.11** respectively. The fabricated limb and V_1-V_2 individual electrodes have the same pattern and structure as V_3 (the electrode with the shortest wire). The %strain values for V_3, V_4, V_5, and V_6 corresponding to **Figure 1.11** are 51.5%, 35.5%, 29.4%, and 32.9% respectively. All 12-lead ECG measurements were performed on a volunteer, with written permission, using MAC® 5000 Resting ECG Analysis device (GE Medical Systems *Information Technologies*, Fl, USA). For comparison purposes, the experiment was repeated using commercial Ag/AgCl ECG electrodes (PRO-TAB/T2334, Bio Protech Inc.), the results of which are shown in **Figure 1.12.**

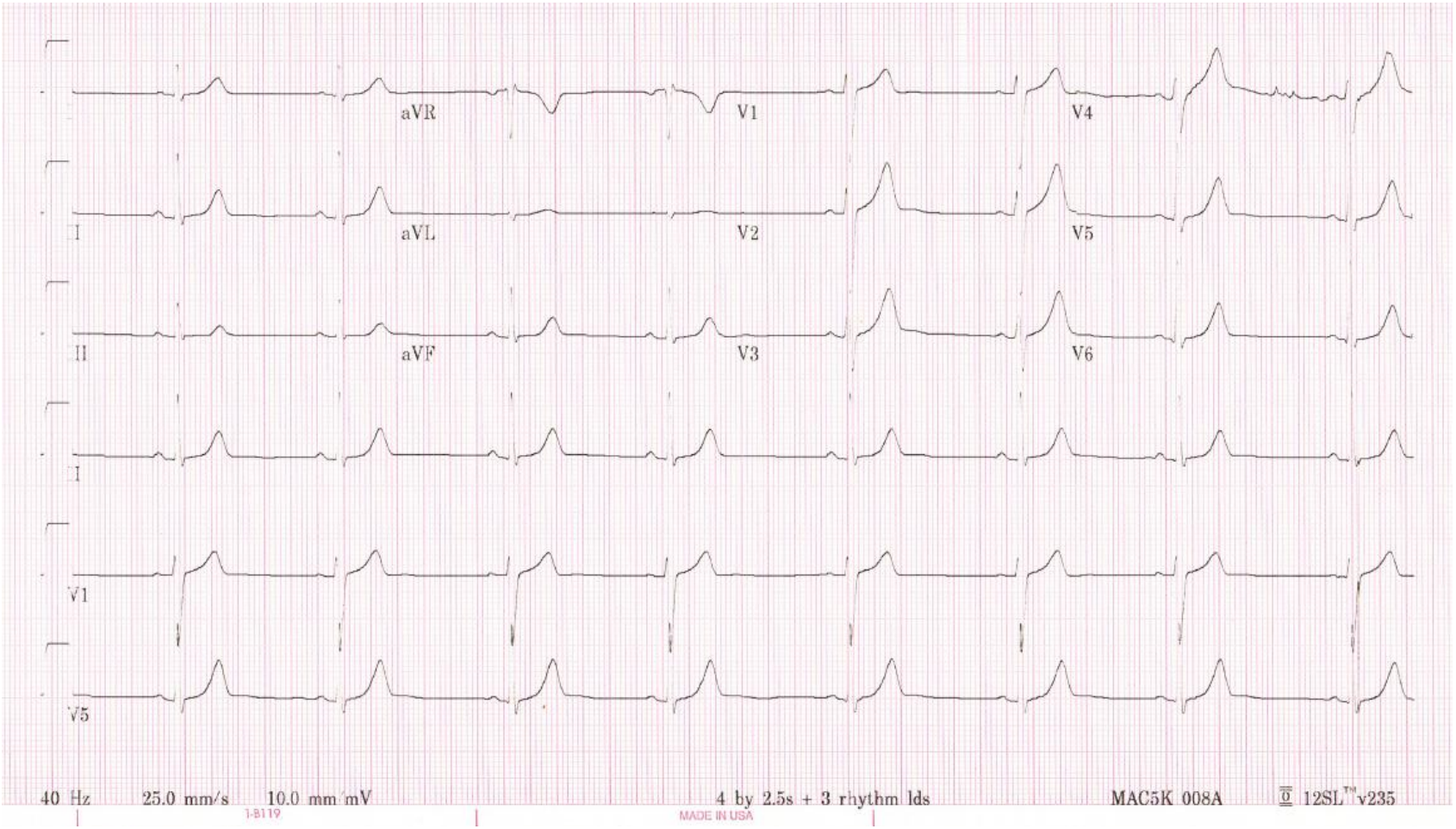

Figure 1.10. 12-lead ECG data collected using fabricated dry electrodes.

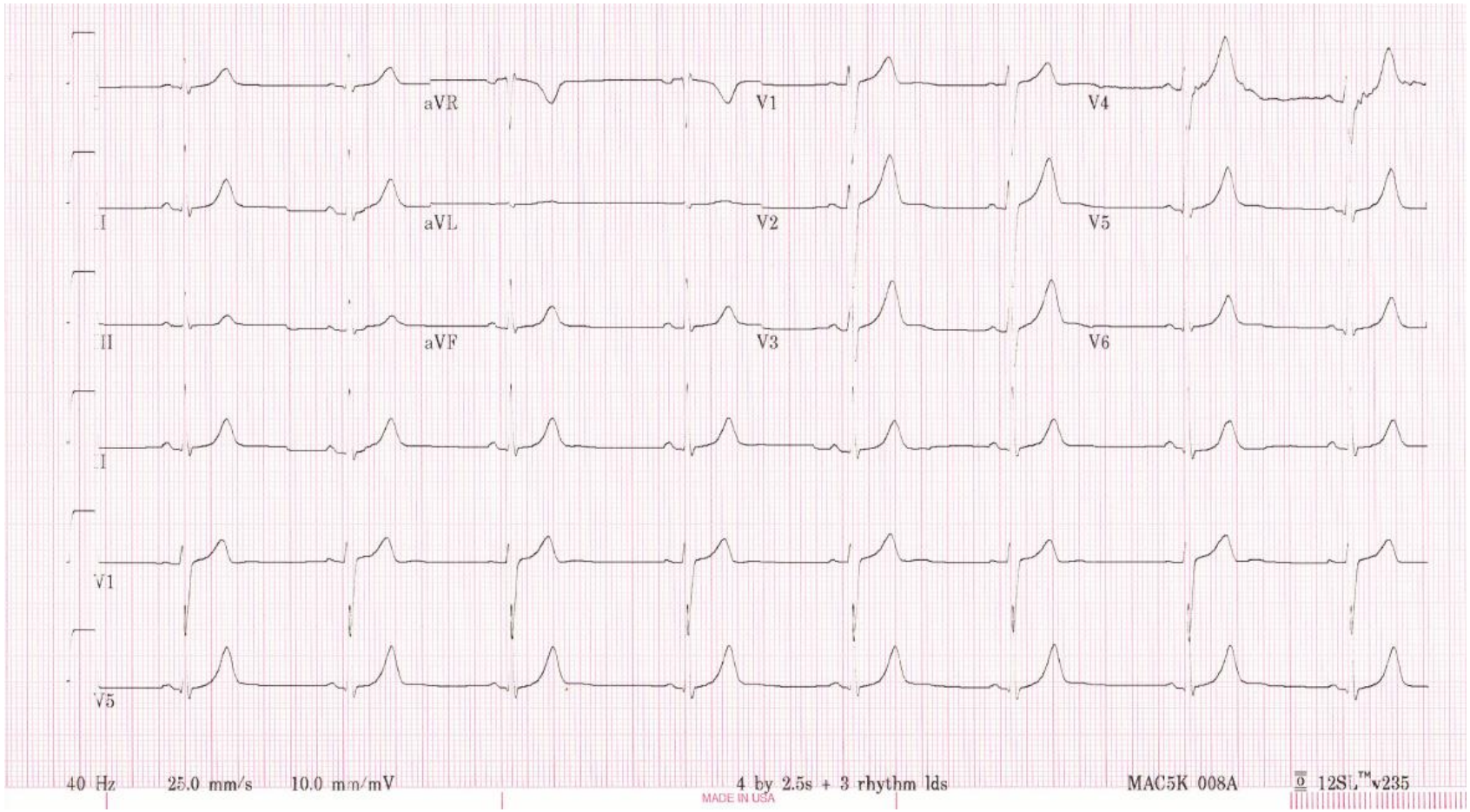

Figure 1.11. 12-lead ECG data collected using fabricated electrodes at ~30% strain for V_3-V_6

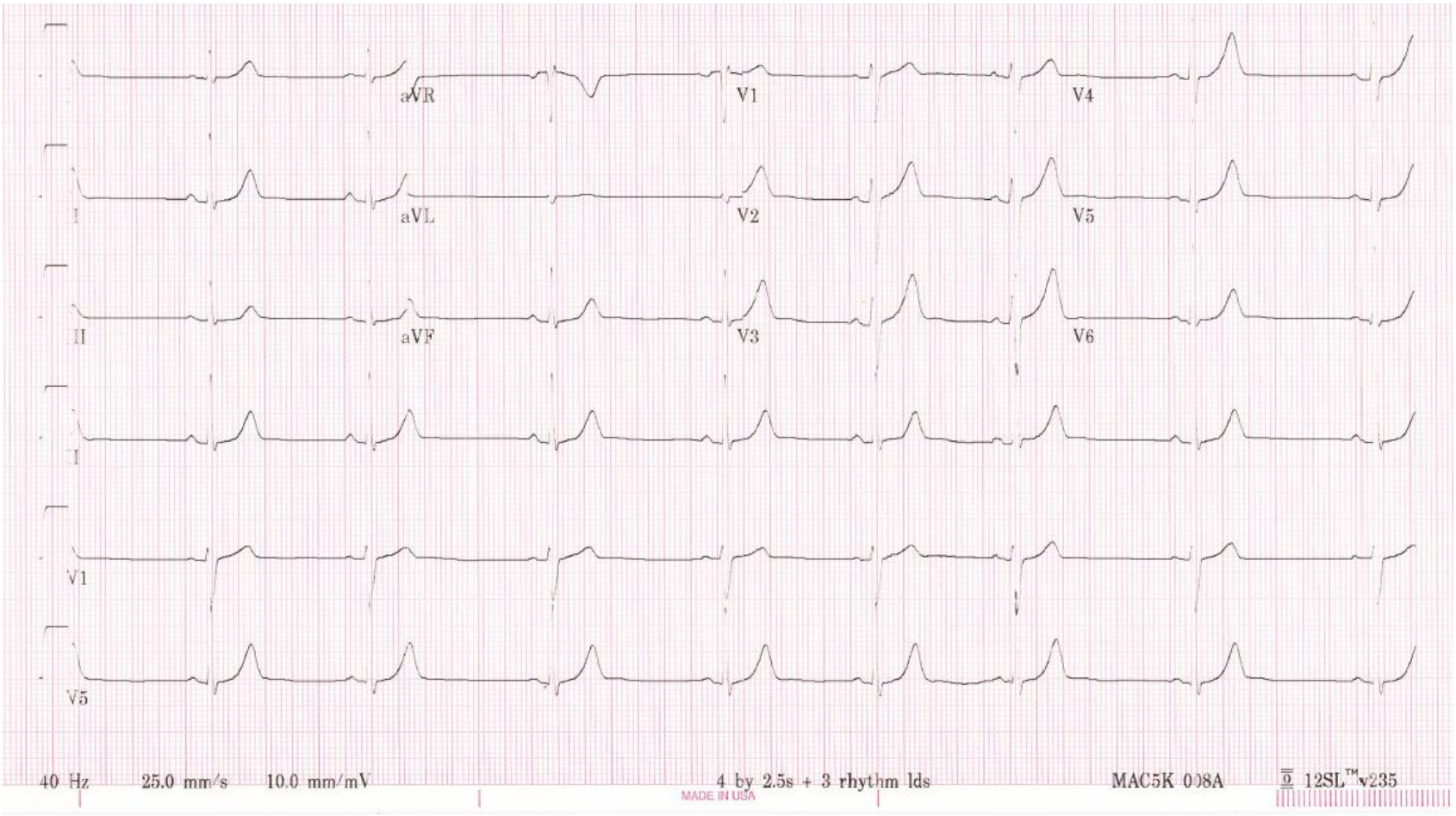

Figure 1.12. 12-lead ECG data collected using commercial electrodes.

In addition to the 12-lead ECG recordings, 3-lead measurements are also commonly used in the research setting. 3-lead measurements were performed in order to numerically characterize the electrode performances. For this recording, electrodes were used such that a reference electrode is placed in the position of V_1, the counter electrode in the position of V_2, and the working electrode takes the place of electrodes in V_3 to V_6 positions one at a time. These measurements were taken place to characterize the four electrodes with different wire lengths (i.e. V_3-V_6) using an OpenBCI Cyton biosensing board. OpenBCI is an open-source brain-computer interface platform with a graphic user interface software that allows for real-time viewing and recording of ECG data.[11]

Figure 1.13 shows the 3-lead ECG measurements taken using commercial electrodes, fabricated V_3-V_6 band, and stretched V_3-V_6 band from left to right respectively. The %strain values corresponding to the wires on the band were each measured after the band was stretched to >30% higher than its original length which resulted in V_3-V_6 wires to stretch to 8.0%, 41.5%, 34.2%, and 33.3% higher than their original length respectively. The collected raw ECG data were then filtered and plotted via MATLAB, and their signal-to-noise ratios (SNR) were calculated. The MATLAB data processing consisted of the following IIR Butterworth filters:

1. an 8^{th} order highpass filter with a cutoff frequency of 0.5Hz,
2. an 8^{th} order notch filter with a stop band frequency of 49-51Hz,
3. and an 8^{th} order notch filter with a stop band frequency of 59-61Hz,

where the highpass filter is used to remove the DC offset and the notch filters are needed to remove the noise due to the powerlines. The SNR values for each electrode were calculated and reported in **Table 1.1**. Each of the following SNR values represent the average of 4 heartbeat SNRs per electrode and were calculated using MATLAB's snr function. This function calculates the SNR by

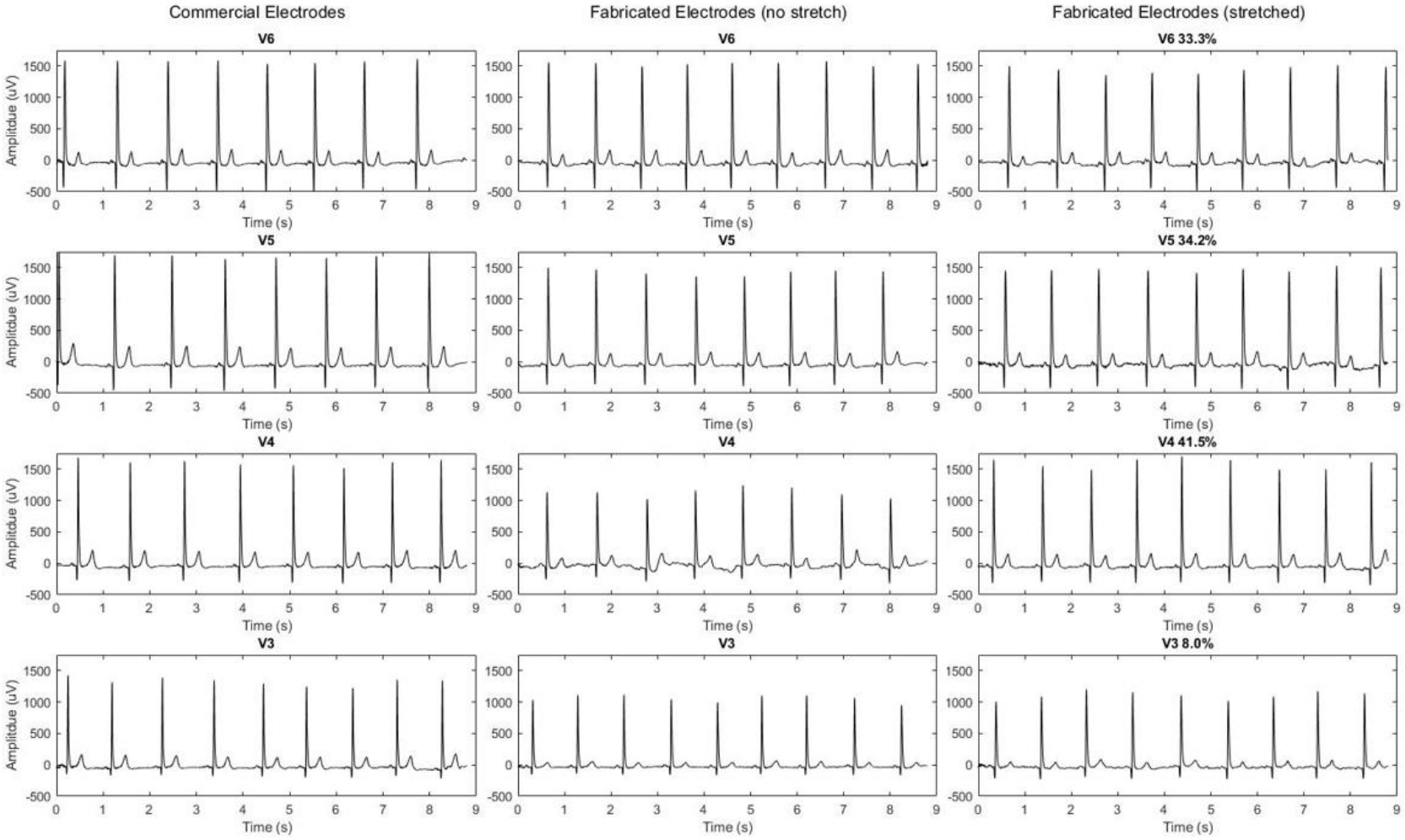

Figure 1.13. 3-lead ECG measurements of commercial, fabricated, and stretched fabricated electrodes are shown from left to right respectively.

computing the ratio of the summed square magnitude of the signal to the that of the noise.[12] The noise was selected as the data points before and after each heartbeat with a size of ½ of the length the heartbeat each (**Figure 1.14**).

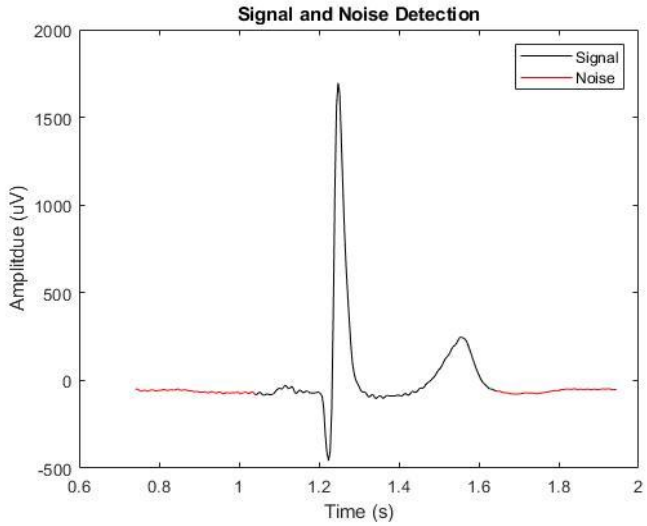

Figure 1.14. The signal and noise data selection for SNR calculation per heartbeat.

Table 1.1. SNR values of the commercial electrodes placed in the positions of V_3 through V_6 and electrodes V_3-V_6 for the fabricated band before and after stretch.

Commercial Electrodes		**V3**	**V4**	**V5**	**V6**
SNR (dB)		13.54	13.89	14.56	17.02
Fabricated Electrodes		**V3**	**V4**	**V5**	**V6**
SNR (dB)	No stretch	14.22	12.94	13.55	14.47
	Stretched	13.33	12.92	14.94	14.05
%Strain		8.00%	41.50%	34.20%	33.30%

1.3.2 Hydrogel Characterization

An adhesive hydrogel formulation was achieved by combining the recipes from Cha et al.[10] and Zhang et al.[13] and adjusting accordingly. Where using $CaCl_2$ as a weak ionic crosslinker for

PVA chains was utilized from Cha et al., and addition of PEDOT:PSS at a 0.14 wt% to increase the conductivity was utilized from Zhang et al.. The characteristics of the fabricated hydrogels were determined using Potential Electrochemical Impedance Spectroscopy (PEIS), the results of which were used for making adjustments in the ratios of the components. The PEIS measurements were performed using SP-200 BioLogic Science Instrument, and EC-Lab Software. Initially, for 0.84g of PEDOT:PSS in the 10wt% PVA solution (0.5g PVA), the amount of $CaCl_2$ was varied from 0.03g to 2.1g. As shown in **Figure 1.15 (a)** and **(b)**, the resistance first decreases as the concentration of $CaCl_2$ is increased, but it reaches saturation at 1.6g. For the PEIS measurements in **Figure 1.15 (b)**, the frequency was ranged from 10mHz to 1KHz with a sinus amplitude of

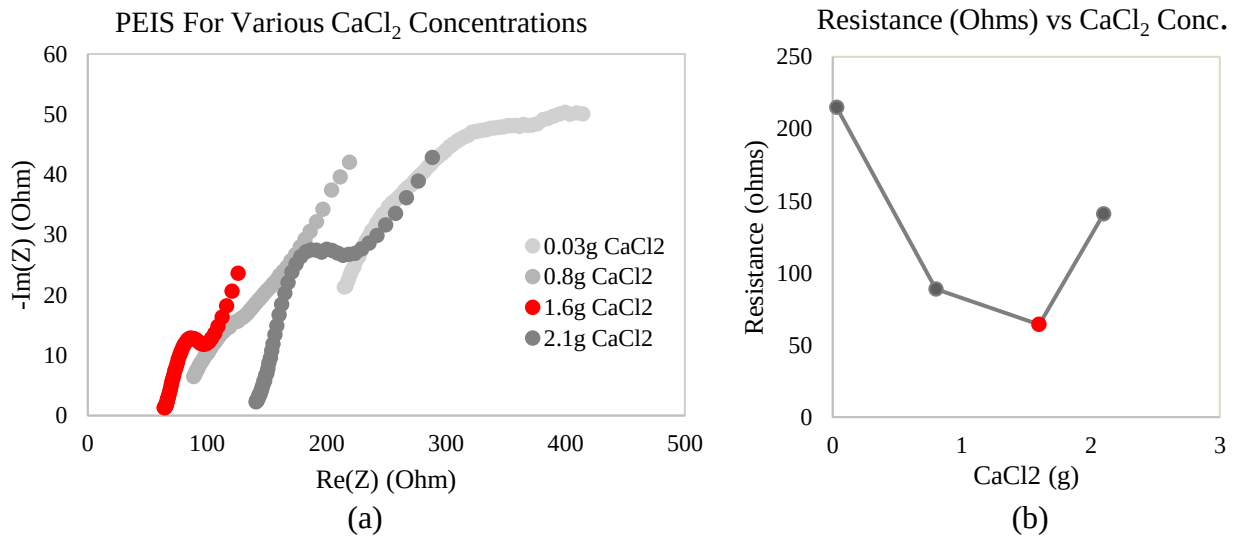

Figure 1.15. (a) The PEIS measurements (b) and resistance of the hydrogel as the $CaCl_2$ concentration is increased.

10mV, and the hydrogel was coated on a microscope slide with two electrodes at 1cm apart. For the hydrogel containing 0.5g PVA (10wt%), 0.84g PEDOT:PSS, and 1.6g CaCl2 (herein referred to as Hydrogel 1) the PEIS and hydrogel mass, as the water evaporated, were recorded over a period of 7 days (**Figure 1.16 (a)** and **(b)** respectively). The results of this experiment indicated

that the amount of residual water remaining in the hydrogel has the most significant reduction during the first day (0.3% reduction) but becomes more stable thereafter, and the resistance increases over time as the drying occurs.

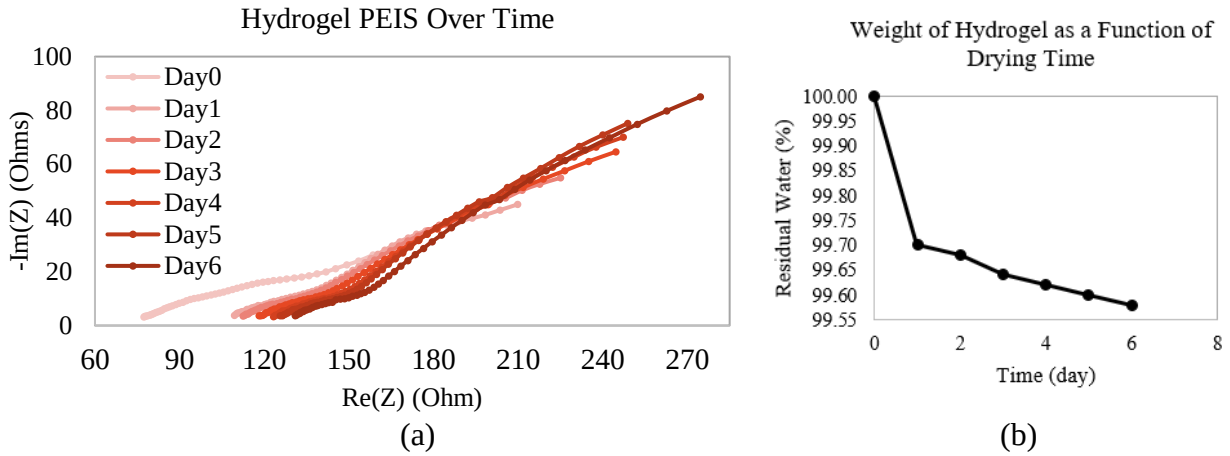

(a) (b)

Figure 1.16. (a) The PEIS measurements (b) and residual weight of Hydrogel 1 as a function of drying time.

The amount of PEDOT:PSS was then doubled (Hydrogel 2) compared to that of in Hydrogel 1; however, the resistance was not reduced unless $CaCl_2$ concentration was also almost doubled (Hydrogel 3). Subsequently, the PVA solution had saturated and increasing either CaCl2 or PEDOT:PSS did not reduce the resistance. The recipes used and PEIS measurements for these trials are shown in **Table 1.2** and **Figure 1.17** respectively.

Table 1.2. The recipes used for hydrogel trials as concentrations of PEDOT:PSS and $CaCl_2$ was varied in the solutions containing 0.5g of PVA dissolved in 4.5g of DI water.

Recipe	**Hydrogel 1**	**Hydrogel 2**	**Hydrogel 3**	**Hydrogel 4**	**Hydrogel 5**
PVA	0.5g	0.5g	0.5g	0.5g	0.5g
PEDOT:PSS	0.8400g	1.546g	1.546g	2.0g	2.0g
CaCl2	1.6g	1.6g	2.1g	2.7g	3.2g

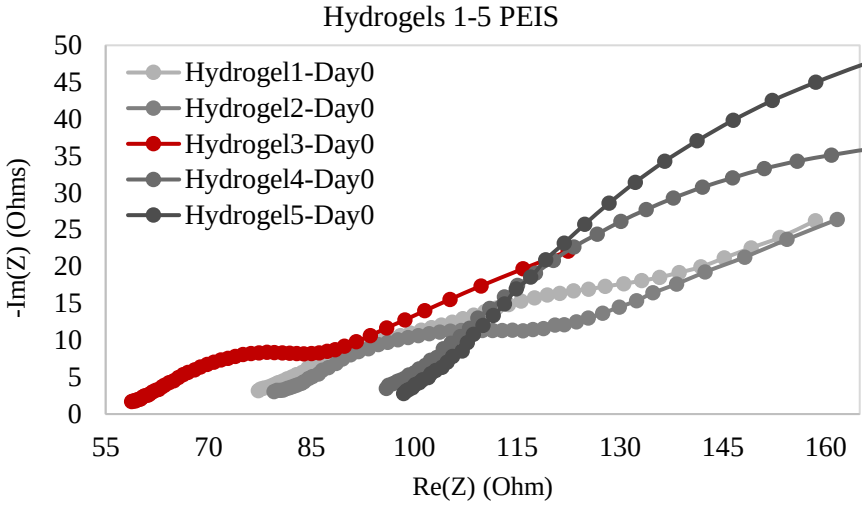

Figure 1.17. PEIS measurements of Hydrogels 1-5.

Considering that the PEIS results from **Figure 1.17** show that Hydrogel 3 has the lowest impedance; this hydrogel was used for ECG measurements and is characterized further. PEIS was measured for Hydrogel 3 (0.5Hz - 1KHz) by coating it on the surface of two fabricated V_3 electrodes, which were then placed on skin at ~3cm apart. The impedance spectroscopy results and the equivalent circuit model (adapted from Muhlsteff and Such [14]) used for data fitting via EC-Lab software are shown in **Figure 1.18 (a)** and **(b)** respectively. In the equivalent circuit model, Q1 accounts for nonidealities in capacitance and can be used to calculate constant phase element (Z_{CPE}) due to the double layer at the electrode-electrolyte interface by

$$Z_{CPE} = \frac{1}{Q}(j\,\omega)^{-n} \quad , \; 0 < n < 1 \tag{1-7}$$

where it repesents an ideal capacitor for n = 1. Moreover, in this figure R1 reperesents the charge transfer resistance at the electrode-electrolyte interface, R2 is the resistance of the hydrogel, and C3 and R3 reperesent the capacitance and resistance of the skin. Compared to the case of PEIS measurement for fabricated dry electrodes (**Figure 1.19**), the electrodes coated with Hydrogel 3 have a considerably lower impedance.

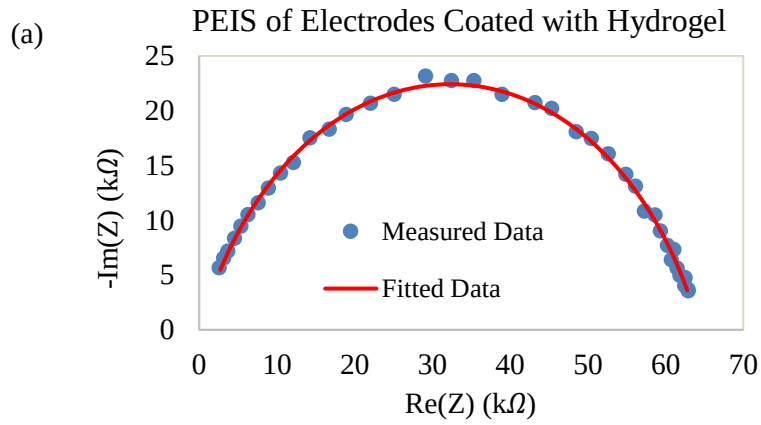

(b)

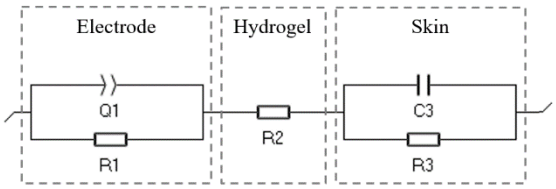

Q1	0.183	$\mu F.s^{n-1}$
n	0.774	
R1	63,700	Ω
R2	125	Ω
C3	8.36	μF
R3	542	Ω

Figure 1.18. (a) PEIS measurement for V_3 electrodes coated with Hydrogel 3 and placed on the skin and (b) its equivalent circuit model.

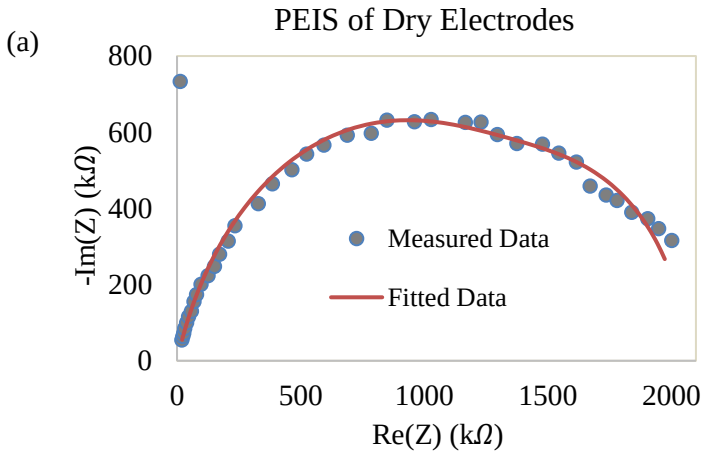

(b)

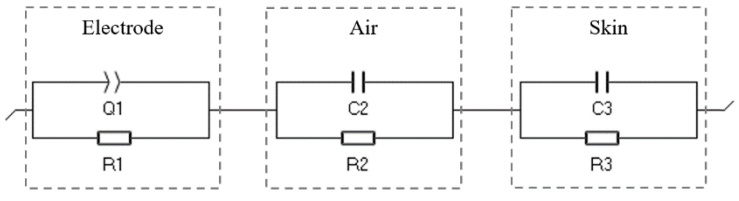

Q1	0.0167	$\mu F.s^{n-1}$
n	0.792	
R1	1,570,000	Ω
C2	0.16	μF
R2	503,000	Ω
C3	8.36	μF
R3	542	Ω

Figure 1.19. (a) PEIS measurement for V_3 dry electrodes placed on the skin and (b) its equivalent circuit model.

Additionally, 3-lead ECG measurements of the V_3-V_6 band were repeated using the electrodes coated with hydrogel, the results of which are shown in **Figure 1.20** and **Table 1.3**. The signal-to-noise (SNR) values reported in **Table 1.3** are measured according to the process describe in section 1.3.1. Compared to the SNR values measured for the fabricated dry electrodes, as shown in **Table 1.1**, there is a slight decrease in SNR of hydrogel coated electrodes. However, as shown in **Figure 1.20**, the hydrogel coated electrodes (**Figure 1.20 (c)**) can detect the ECG waveforms with a comparable quality.

Table 1.3. SNR values of V_3-V_6 electrodes coated with hydrogel for the fabricated band.

Fabricated Electrodes w/ Hydrogel	**V3**	**V4**	**V5**	**V6**
SNR (dB)	13.40	12.78	13.23	13.87

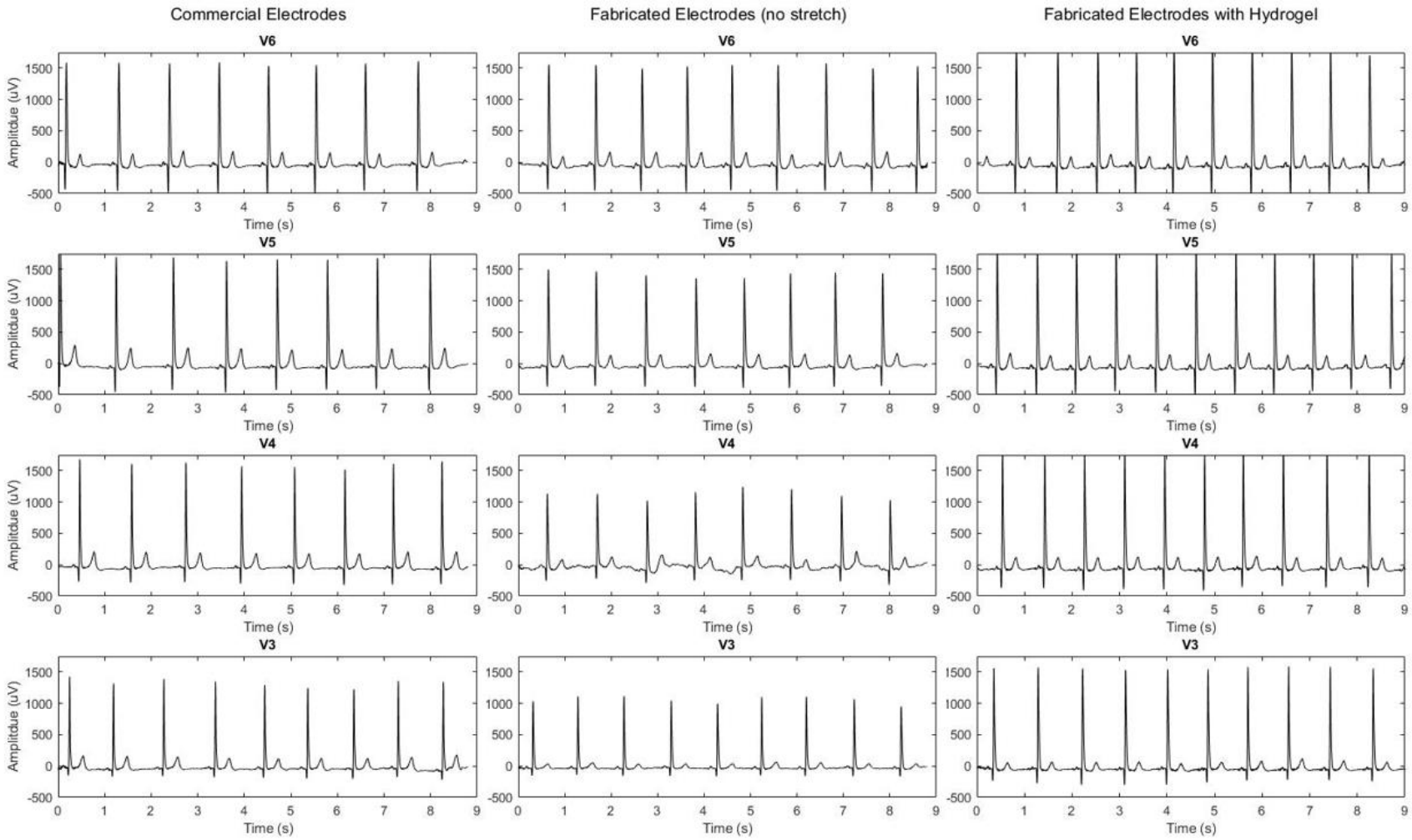

Figure 1.20. 3-lead ECG measurements of commercial and fabricated dry and with-hydrogel electrodes are shown from left to right respectively.

1.4 Conclusion and Future Directions

The fabricated dry and with-hydrogel electrode band containing V_3 to V_6 electrodes and their corresponding wires are capable of recording ECGs and can provide a fast and more accurate electrode placement as opposed to the conventional single electrodes. Hence this prototype can be used to improve the electrocardiography process for clinical diagnosis. This prototype can be further improved by integrating of the entire ten electrodes used in a 12-lead ECG into a stretchable fabric in the same manner. Additionally, a second crosslinker can be added to the hydrogel to speed the crosslinking process of this component.

1.5 References

1. Zhang S. Cardiac conduction system. McMaster Textbook of Internal Medicine. empendium. https://empendium.com/mcmtextbook/image/B31.031_6254. Accessed November 20, 2020.

2. Sörnmo L, and Laguna P. Bioelectrical Signal Processing in Cardiac and Neurological Applications. *Elsevier Inc.*. 2005.

3. Rajaganeshan R, Ludlam C L, Francis D P, Parasramka S V, Sutton R. Accuracy in ECG lead placement among technicians, nurses, general physicians and cardiologists. *Int J Clin Pract.*. 2008;62(1):65-70.

4. Kania M, Rix H, Fereniec M, Zavala-Fernandez H, Janusek D, Mroczka T, Stix G, Maniewski R. The effect of precordial lead displacement on ECG morphology. *Med Biol Eng Comput*. 2014;52(2):109-119.

5. Kerwin A J, McLean R, Tegelaar H. A method for the accurate placement of chest electrodes in the taking of serial electrocardiographic tracings. *Can Med Assoc J*. 1960;82(5):258-261.

6. Ecoflex TM Series. Smooth-On. Accessed November 29, 2020. https://www.smooth-on.com/tb/files/ECOFL EX_SERIES_TB.pdf

7. Yin L, Seo J K, Kurniawan J, Kumar, R, Lv, J, Xie, L, Liu X, Xu S, Meng Y S, Wang J. Highly Stable Battery Pack via Insulated, Reinforced, Buckling-Enabled Interconnect Array. *Small*. 2018;14(43):e1800938.

8. Wang K, Parekh U, Pailla T, Garudadri H, Gilja V, Ng T N. Stretchable Dry Electrodes with Concentric Ring Geometry for Enhancing Spatial Resolution in Electrophysiology. *Adv Healthc Mater*. 2017;6(19):10.1002/adhm.201700552.

9. Jiang S, Liu S, Feng W. PVA hydrogel properties for biomedical application. *J Mech Behav Biomed Mater*. 2011;4(7):1228-1233.

10. Cha W, Hyon S, Graiver D, Ikada Y. Sticky Poly (vinyl Alcohol) Hydrogels. *J Appl Polym Sci.* 1993;47:339-343.

11. OpenBCI. Accessed November 29, 2020. https://openbci.com.

12. snr. The Mathworks, Inc.. Accessed November 29, 2020. https://www.mathworks.com/help/signal/ref/snr.html.

13. Zhang Y, Guo M, Zhang Y, Tang C Y, Jiang C, Dong Y, Law W, Du F. Flexible, stretchable and conductive PVA/PEDOT:PSS composite hydrogels prepared by SIPN strategy. *Polym Test*. 2020;81:106213.

14. Mühlsteff J, Such O. Dry electrodes for monitoring of vital signs in functional textiles. *Proc. of the 26th Annual International Conference of the IEEE Engineering in Medicine and Biology Society (EMBS `04)*, San Francisco, CA, USA. 2004;2212-2215.

Chapter 2

Printing of the Passivation Layer in an All-Printed Supercapacitor

2.1 Introduction

A reliable and efficient energy storage device is essential to operate the electrical systems and to store the energy harnessed for many applications such as during a space mission. On-demand fabrication of an energy storage device offers versatility for variable power needs and supplements the capabilities of In-Space Manufacturing (ISM) during long-duration space missions. Of such devices, supercapacitors have a high power density and a long lifespan rendering them advantageous for the frequent energy use during space missions. Manufacturing of supercapacitors by printing allows for ease of customization and reproducibly of the device.

An end-to-end printing of an in-plane supercapacitor has been previously demonstrated by Seol et. al.[1] The layers of this supercapacitor were printed by sequential additive manufacturing

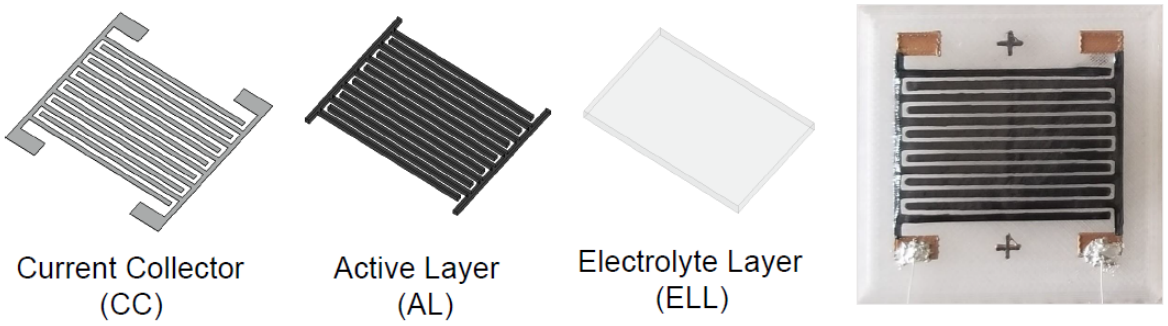

Figure 2.1. Printed supercapacitor layers.

process, and consisted of a 3D-printed substrate, current collector, active layer, and gel polymer electrolyte, where the current collector and active layer are composed of an interdigitated pattern (**Figure 2.1)**.[1]

To increase the lifetime and stability of such device, a suitable material was identified for its passivation, and a printing mechanism was developed for this layer. Without passivation, the cyclic voltammetry measurements of the device show that the device starts to gradually degrade by day 7 and completely deactivates by day 14, as shown in **Figure 2.2**.[2]

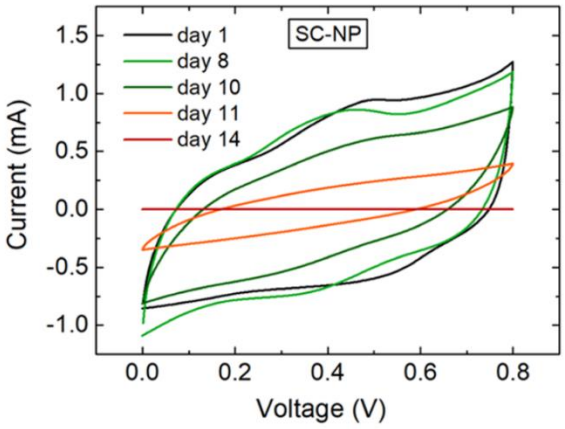

Figure 2.2. Non-passivated device over time.[2]

2.2 Methods

The supercapacitors were first printed using the sequential additive manufacturing process as established by Seol et. al.[1] A series of widely known low-reactive polymers that are commercially available were then examined for their feasibility to protect the supercapacitor from the ambient: Polytetrafluoroethylene (Teflon), Polyvinyl (PV) Alcohol, Polyvinyl (PV) Acetate (wood glue), PV Acetate mixed with electrolyte, and UV-curable Cycloaliphatic epoxy (CE). The passivation materials were individually printed on supercapacitors via Voltera V-One PCB printer. The printer is shown in **Figure 2.3**.

The printing pattern for the passivation layer was developed using AutoCAD, and as shown in **Figure 2.4**, it is consisted of two main steps. In the first step (**Figure 2.4 (a)**), with the Voltera nozzle close to the substrate, only the area surrounding the supercapacitor is printed with passivation material. In the second step, the nozzle height level is increased to avoid any collusion with the electrolyte layer, and then the material is printed on the entire inner area containing the functioning layers (**Figure 2.4 (b)**). In the case of CE, the outermost layer in **Figure 2.4 (a)** is first printed and cured with UV-light prior to proceeding with the rest of the pattern. This is to avoid

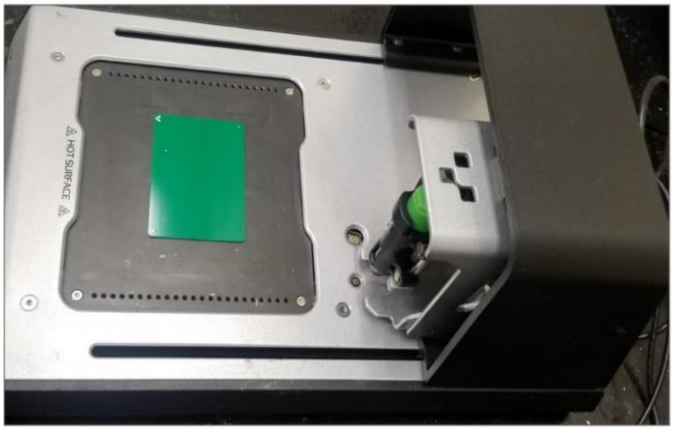

Figure 2.3. Voltera V-One PCB printer.

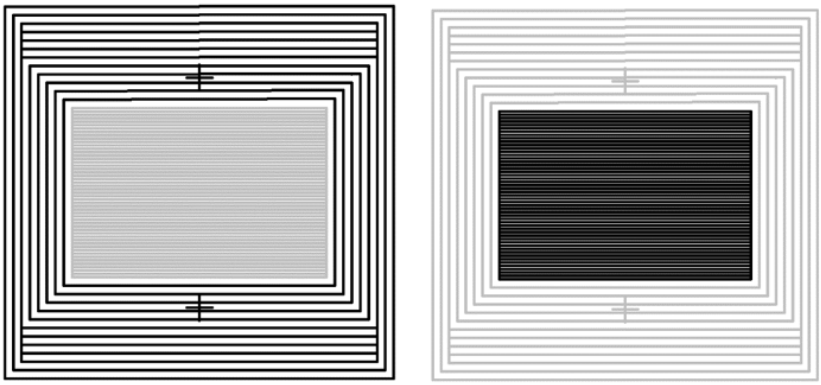

(a) (b)

Figure 2.4. The two main steps for printing of the passivation layer. (a) The outer layer (left) is printed first, and then (b) the supercapacitor surface is covered.[2]

overflow of CE from occurring, and acts as a barrier. Additionally, the supercapacitor coated with CE was cured for 15 minutes in UV light after printing was completed.

2.3 Effectiveness of the Passivation Layer

The printed passivation layers were characterized in terms of their ability to preserve the device over time and not react with the electrolyte later. For this purpose, cyclic voltammetry (CV)

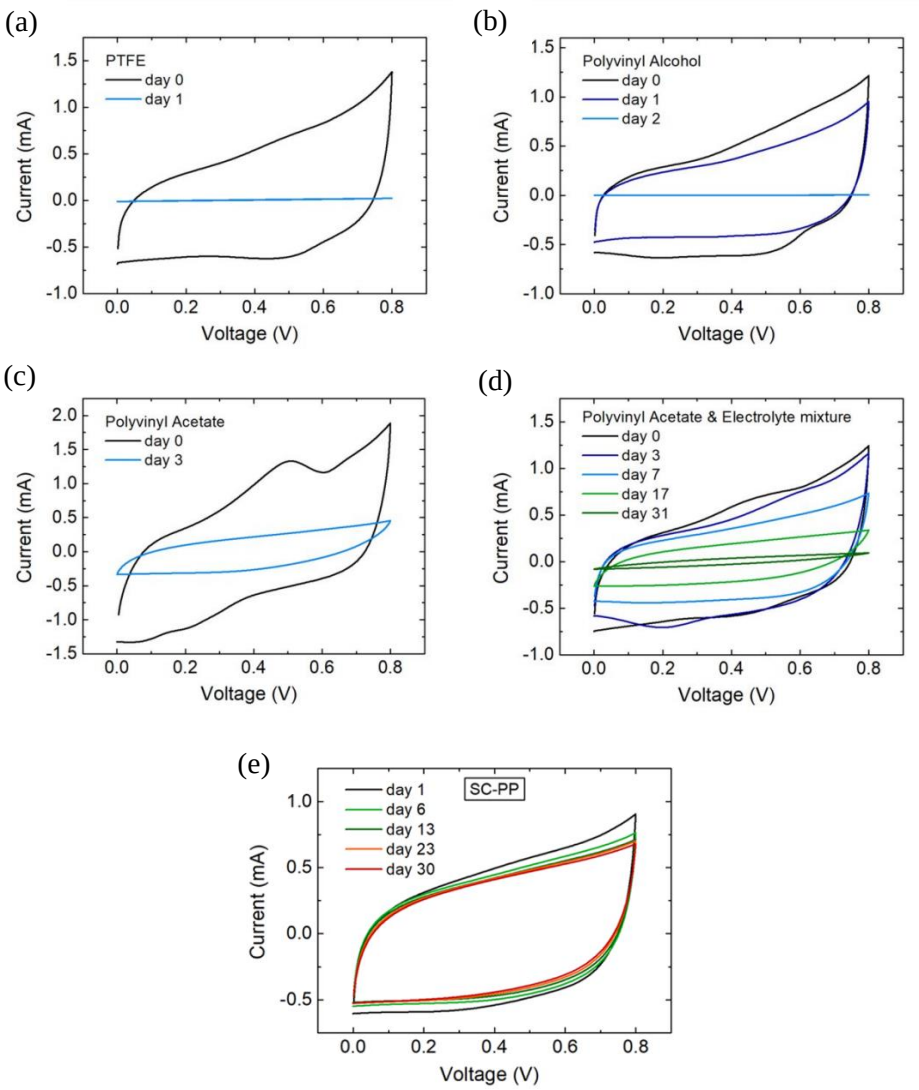

Figure 2.5. The effectiveness of the printed passivation layers for devices with (a) PTFE, (b) PV alcohol, (c) PV acetate, (d) PV acetate & electrolyte, and (e) CE as their preserving material shown in terms of CV measurements.[2]

of the devices with different materials used as the passivation layer was performed. For the materials tested, CV of the devices were measured before and after addition of the passivation layer. In the cases of PTFE and PV alcohol, the devices were deactivated by up to two days after printing due to shrinkage of these material upon drying which resulted in dislocation of the active and current collector layers, as shown in **Figure 2.5 (a)** and **(b)**. Furthermore, PV Acetate reacted with the electrolyte and reduced its ion conductivity even after it was partially mixed with the electrolyte prior to being deposited, **Figure 2.5 (c)** and **(d)**. However, in the case of CE, the material successfully preserved the device as it significantly reduces the penetration of water and oxygen molecules, and it did not react with the electrolyte. The effectiveness of CE as a passivation material was further investigated using density functional theory by Dr. Seol, and the results showed that its effectiveness is due to the existence of the positive energy barrier at the adhesion points along the diffusion pathway of water and oxygen through CE. [2]

2.4 Conclusion and Future Directions

Printed Cycloaliphatic epoxy has shown an excellent ability in preserving of the printed supercapacitors even on day 30 after the device fabrication. Therefore, a feasible method for improving the lifetime and stability of an all-printed supercapacitor has been demonstrated. Additionally, a printing procedure was established for CE, which can be applied to curable material with the same viscosity, such as Ecoflex. As established in Chapter 1, Ecoflex is used as both the backbone and insulation layer for the ECG electrode prototype proposed in this thesis, and the conductive electrode has a similar consistency and material as the current collector layer of the supercapacitor. Therefore, the ECG electrode band can be fabricated using the same process that has been established for printing of the supercapacitors.

Chapter 2, in full, is the reprint of the material as it appears in the publication: Myeong-Lok Seol, Ellie Sadatian, Seohyeon Jang, Curtis Hill, Inho Nam, Jin-Woo Han, and M. Meyyappan, “Printing of a Passivation Layer for the Protection of Printed Supercapacitors”, *ACS Appl. Electron. Mater.* 2, 3643 (2020). The thesis author is the primary author of this thesis and second author of this paper.

2.5 References

1. Seol M.-L, Nam I, Ribeiro E L, Segel B, Lee D, Palma T, Wu H, Mukherjee D, Khomami B, Hill C, Han J-W, Meyyappan M. All-Printed In-Plane Supercapacitors by Sequential Additive Manufacturing Process. *ACS Appl. Energy Mater.* 2020;3:4965−4973.

2. Seol M.-L, Sadatian E, Jang S, Hill C, Nam I, Han J-W, Meyyappan M Printing of a Passivation Layer for the Protection of Printed Supercapacitors. *ACS Appl. Electron. Mater.* 2020;2:3643−3649.

Chapter 3

Capacitive Pressure Sensing via Distributed Multi-Channel Frequency-Modulation-Based System

3.1 Introduction

Capacitive pressure sensors have many applications in medical devices and wearable electronics, such as use in gloves for quantification of neuromuscular disorder.[1] In such applications, an array of sensors distributed over a large surface is needed which makes the use of a distributed multi-channel frequency-modulation-based analog-to-digital convertor (FM-ADC) a suitable method as it offers an integration of and acquisition from a multitude of sensors.[2-4] This technique also minimizes the number of ADC convertors needed for data acquisition in an N-channel sensor system from N to a one ADC, which in turn lowers the power consumption of the system.

The FM-ADC system works by modulating the frequency of a frequency modulated (FM) carrier wave based on the applied pressure on the capacitive pressure sensing transducer. The FM carrier wave is first generated using a voltage-controlled oscillator (VCO). The VCO topology used features a cross-coupled current reuse LC tank from Yun et. al.[5], **Figure 3.1**. The capacitive transducer is connected to the tank of the VCO, which can then directly change the VCO oscillation frequency based on the pressure applied. This capacitive transducer was originally designed and fabricated by Amit et. al. and is consisted of a parallel plate capacitor with flexible screen-printed electrodes and porous PDMS dielectric. [6]

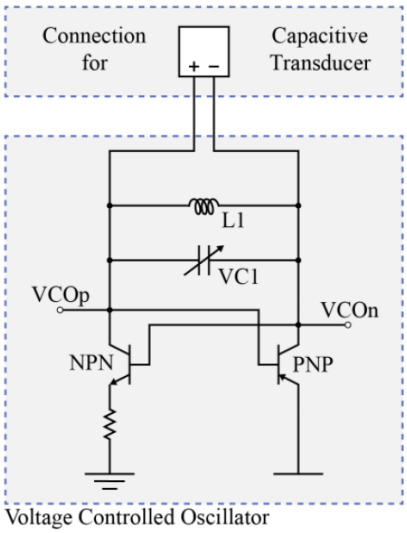

Figure 3.1. Schematic of the cross-coupled current reuse LC tank voltage-controlled oscillator used for FM carrier generation.

Using this technology as a basis, a printed circuit board (PCB) was developed for acquisition and quantification of an applied pressure.

3.2 Front-End Circuit Design

A bandpass amplifier (BPA), was designed to drive the output carrier from the VCO onto the system's frequency-domain-multiplexed (FDM) bus. The BPA, as shown in **Figure 3.2**, was

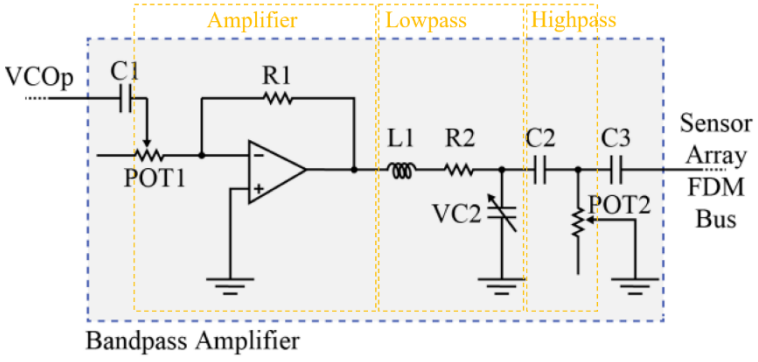

Figure 3.2. Schematic of the bandpass amplifier used for signal combination on the FM-FDM bus.

composed of amplification, low filter, and high pass filter sections, and it was made such that its center frequency and gain can be adjusted via POT2 potentiometers and VC2 variable capacitor.

Complete with low dropout regulators (LDO), which isolate the power supplies of the sensors, a PCB was designed using Altium, and the product was assembled using discrete off-the-shelf commercial parts, **Figure 3.3**. The tank inductor is a 100 μH 0603 inductor that was chosen for its low series resistance (5.5 ohms), which contributes to low oscillator power and phase noise. Additionally, the operational amplifier employed is a Texas Instruments OPA835, chosen for its low power consumption while satisfying gain-bandwidth requirements.

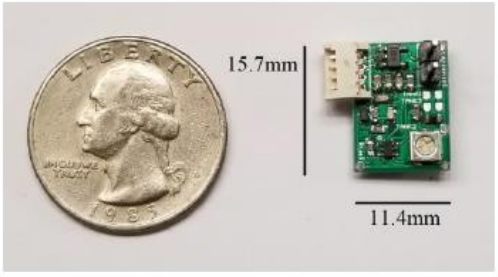

Figure 3.3. Assembled sensor PCB.

3.3 Experimental Testbed and Pressure Detection

The sensor board was provided 5.5V DC power via a Keithley 2230G bench power supply, and its analog output was acquired via a Measurement Computing USB-2020 data logging device. The sensor frequency of carrier oscillation was determined by Fast Fourier Transform (FFT) of the data via MATLAB and subsequent peak detection. The 8 megasample/second acquisition rate of the USB-2020 is less than the true oscillation frequency of the VCO in the sensor electronics (~12.5MHz) so the detected signal is folded back into the first Nyquist zone via subsampling; this means that an increase in detected frequency corresponds to a decrease in true oscillation frequency.

The capacitive pressure sensing transducer was placed on a digital scale on the print surface of a modified Alunar M508 3D printer. The 3D printer's movable head was outfitted with a flat probe surface to ensure consistent computer-controllable pressure on the transducer during measurement. It also allowed for progressively increasing and decreasing applied pressure without removal of pressure in between measurements, which is a critical test platform requirement for accurate transducer characterization.

This test platform, **Figure 3.4**, was used to compress the capacitive pressure transducer as the z-axis of the printer was lowered by increments of 0.1 mm, starting with zero compression. For each z-axis increment, the pressure applied to the capacitor was recorded from the digital scale's readout in grams and the center frequency of the sensor board's output was recorded from MATLAB. Once maximum compression was achieved, the z-axis was then raised in increments of 0.1 mm and data points recorded as the compression on the transducer was reduced incrementally back to zero. Time between each measurement was approximately 10 seconds.

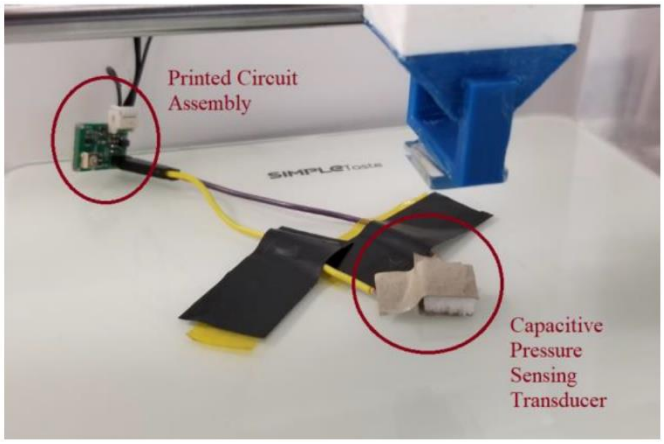

Figure 3.4. Experimental testbed.

This process repeated for 5 trials yields 5th-order polynomial best-fit curves for compression and decompression presented in **Figure 3.5**. Between trials, a maximum deviation in

frequency of 0.879% was observed. The transducer exhibits some hysteresis which is due to the foam's inherent "memory" and the fact that it takes the foam some time to expand and settle following a state of being compressed. With further characterization of the transducer, this hysteresis could be accounted for during real-time measurements with the platform.

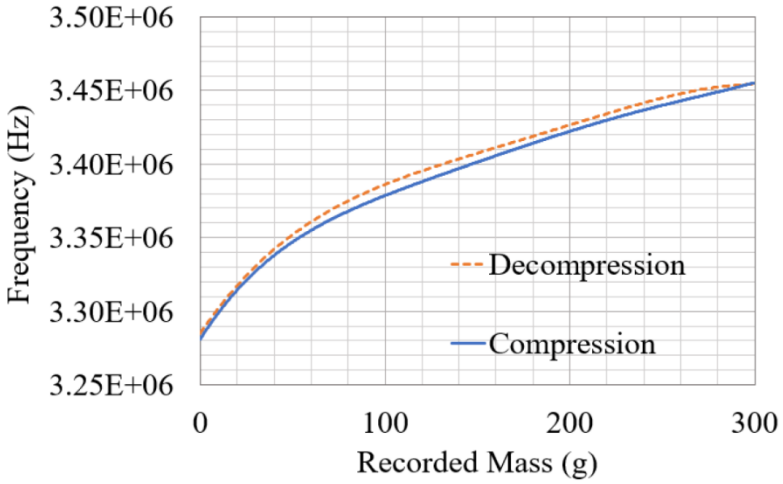

Figure 3.5. Measurement results under increasing and decreasing pressure applied to sensor.

To demonstrate multi-channel operation, two sensor assembly boards were fabricated and connected via their outputs to the common FM-FDM. The FM carrier frequency of each board's output was plotted over time as their transducers were pressed one at a time and then together. The resulting FM carrier frequency versus time plot is shown in **Figure 3.6 (a)** and demonstrates that the pressure signals of individual sensor assemblies are independently detectable in a multi-channel system (**Figure 3.6 (b)**).

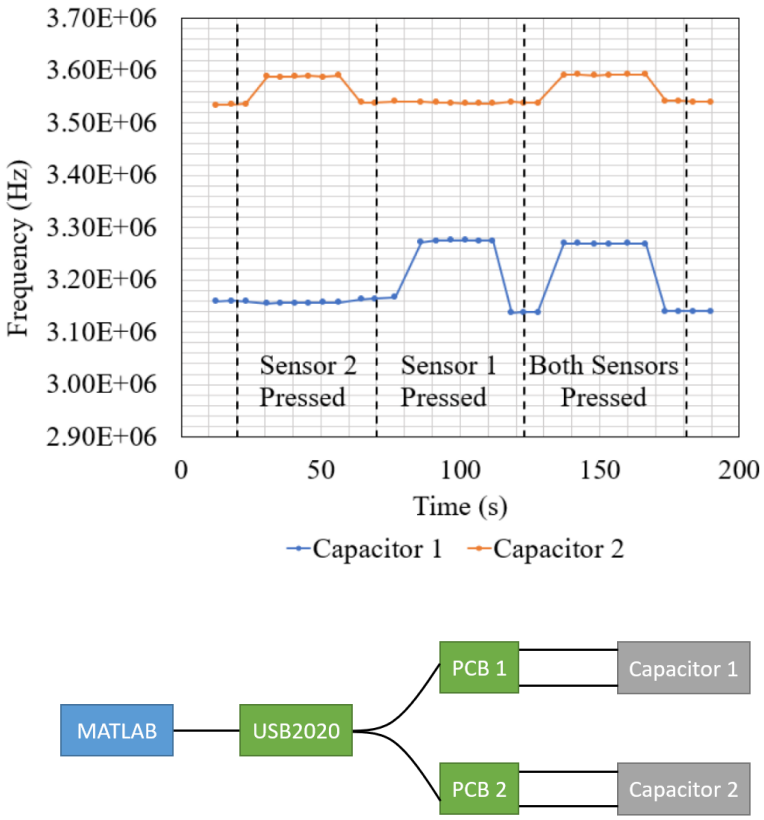

Figure 3.6. (a) Measurement results for two-channel test and (b) its overall system setup.

3.4 Conclusion and Future Directions

The described distributed multi-channel FM-ADC data acquisition system has demonstrated the ability to detect, transfer, and distinguish the data incoming from the changes made to input capacitive pressure sensors. Additionally, this system can be used with other sensor types used in wearable electronics as the system is sensor-type-agnostic and can digitized the output of sensors with different modalities together. Therefore, this system can be used for other sensors and applications such ECG acquisition. Using a distributed FM-ADC system with 10 channels containing electrodes described in chapter 1, a 12-lead ECG measurement can be acquired which minimizes the amount of wiring and eliminates its associated misconnection of

wires due to user error. This is because after implementation of the PCBs on the electrode band, the data can be transferred with just one wire from the overall system.

3.5 References

1. Jonnalagedda P, Deng F, Douglas K, Chukoskie L, Yip M, Ng T N, Nguyen T, Skalsky A and Garudadri H. An instrumented glove for improving spasticity assessment. *IEEE Healthcare Innovation Point-Of-Care Technologies Conf. - (HI-POCT)*, Cancun, Mexico. 2016;167–170.

2. Warchall J, Kaleru S, Jayapalan N, Nayak B, Garudadri H, Mercier P P. A 678-μW Frequency-Modulation-Based ADC With 104-dB Dynamic Range in 44-kHz Bandwidth. *IEEE Transactions on Circuits and Systems II: Express Briefs*, 2018: 65(10);1370-1374.

3. Warchall J, Theilmann P, Ouyang Y, Garudadri H, Mercier P P. 22.2 A Rugged Wearable Modular ExG Platform Employing a Distributed Scalable Multi-Channel FM-ADC Achieving 101dB Input Dynamic Range and Motion-Artifact Resilience. *2019 IEEE International Solid- State Circuits Conference - (ISSCC)*, San Francisco, CA, USA. 2019;362-364.

4. Warchall J, Balakrishnan A, Balkan Ö, Mercier P P, Garudadri H, Hairston W D, Theilmann P. A multi-channel EEG system featuring single-wire data aggregation via FM-FDM techniques. *2016 IEEE International Symposium on Circuits and Systems (ISCAS)*, Montreal, QC, Canada. 2016;526-529.

5. Yun S-J, Shin S-B, Choi H-C, Lee S-G. A 1mW current-reuse CMOS differential LC-VCO with low phase noise. *2005 IEEE International Solid- State Circuits Conference - (ISSCC)*, San Francisco, CA, USA. 2005;540-616

6. Amit M, Mishra R K, Hoang Q, Galan A M, Wang J, and Ng T N. Point-of-use robotic sensors for simultaneous pressure detection and chemical analysis. *Mater Horiz*, 2019;6:604 - 611.